Unifying the Sørensen-Mølmer gate and the Milburn gate with an optomechanical example

Yue Ma,* Manuel C. C. Pace, and M. S. Kim
QOLS, Blackett Laboratory, Imperial College London, London SW7 2AZ, United Kingdom

(Received 11 February 2022; accepted 27 June 2022; published 11 July 2022)

The Sørensen-Mølmer gate and Milburn gate are two geometric phase gates, generating nonlinear self-interaction of a target mode via its interaction with an auxiliary mechanical mode, in the continuous- and pulsed-interaction regimes, respectively. In this paper we aim at unifying the two gates by demonstrating that the Sørensen-Mølmer gate is the continuous limit of the Milburn gate, emphasizing the geometrical interpretation in the mechanical phase space. We explicitly consider imperfect gate parameters, focusing on relative errors in time for the Sørensen-Mølmer gate and in phase angle increment for the Milburn gate. We find that, although the purities of the final states increase for the two gates upon reducing the interaction strength together with traversing the mechanical phase space multiple times, the fidelities behave differently. We point out that the difference exists because the interaction strength depends on the relative error when taking the continuous limit from the pulsed regime, thereby unifying the mathematical framework of the two gates. We demonstrate this unification in the example of an optomechanical system, where mechanical dissipation is also considered. We highlight that the unified framework facilitates our method of deriving the dynamics of the continuous-interaction regime without solving differential equations.

DOI: 10.1103/PhysRevA.106.012605

I. INTRODUCTION

Utilizing the geometric phase [1,2] in quantum computation was first proposed [3–6] and experimentally realized [7,8] in the platform of trapped ions, making use of the accumulated phase that equals the enclosed area of the closed loop traversed in a phase space satisfying the basic quantum-mechanical commutator $[\hat{X}, \hat{P}] = i$ [9]. Due to its ability to generate an effective interaction between noninteracting subsystems [10], the idea has been widely applied for simulating qubit gates in a variety of physical systems, including quantum optics [11] and superconducting circuits [12]. The geometric phase has also been exploited in optomechanical systems, where a bosonic optical field mode interacts with a mechanical oscillator via radiation pressure [13]. The effective nonlinear self-interaction induced by the geometric phase facilitates generation of the nonclassical field [14] and oscillator [15] states and even the detection of potential quantum gravitational effects [16].

Among the first proposals of the geometric phase gate, the Sørensen-Mølmer gate [4] works in the continuous-interaction regime while the Milburn gate [3] is in the pulsed-interaction regime. In both cases, the collective vibrational motion of the ions is only virtually excited, thus relaxing the requirement of vibrational ground-state cooling. However, this is true only if the mechanical-phase-space trajectory forms a closed loop. It has been pointed out in Ref. [5] that, in the weak-field coupling limit, the internal state of the ions is independent of the state of the collective vibrational motion for any interaction time. In the mechanical-phase-space picture, this can be understood as follows. In the limit of an infinitesimal circle, we can hardly distinguish between open and closed loops. The total enclosed area is kept finite by traversing the phase space infinitely many times. Three natural questions follow. Given that, in the Sørensen-Mølmer gate, the interaction time is subject to an error, which cannot be directly measured and compensated, the mechanical-phase-space trajectory is no longer closed. In this case, will the transformation of reducing the size of the phase-space loop together with traversing the phase space multiple times improve the gate performance? Will the same method help improve the performance of the Milburn gate? How are the behaviors of the two gates connected with each other?

In this paper we explicitly study these questions mentioned above. We consider the Sørensen-Mølmer gate as a continuous-interaction model between a target mode and an auxiliary mechanical oscillator mode, in the form described in Ref. [5] but without restricting it to a trapped ion system. We consider the Milburn gate as a series of pulsed interactions between a target mode and an auxiliary mechanical oscillator mode. We illustrate geometric interpretations of the two gates in the mechanical phase space. We explicitly show how the Sørensen-Mølmer gate is equivalent to the continuous limit of the Milburn gate. We then consider imperfect gates, with a relative time error for the Sørensen-Mølmer gate and a phase error for the Milburn gate. We study the transformation of decreasing the size of the loop together with traversing the phase space multiple times. The purity of both gates increases, but the fidelities of the two gates behave differently. We show that the difference in the fidelity is because the continuous limit of the pulsed scheme involves an error-dependent interaction strength. Finally, we illustrate the analysis using an optomechanical system as an example [17–19], including the dissipation of the mechanical oscillator. We derive analytical solutions of the system in the pulsed-interaction regime and

*y.ma16@imperial.ac.uk

further obtain the results in the continuous-interaction regime by taking the continuous limit without solving differential equations. The results enrich our understanding of the unification of the two interaction regimes.

II. ORIGINAL GATES

We briefly recapitulate the original Sørensen-Mølmer gate and the Milburn gate in a trapped ion system. The Sørensen-Mølmer gate [5] uses bichromatic laser fields to excite the ions, which are slightly detuned from the upper and lower sidebands of a collective center-of-mass vibrational mode of the ions. In the Lamb-Dicke regime, the interaction Hamiltonian corresponds to a unitary time-evolution operator in the form of $\hat{U}(t) = \exp[-iA(t)\hat{J}_y^2]\exp[-iF(t)\hat{J}_y\hat{x}]\exp[-iG(t)\hat{J}_y\hat{p}]$, where $\hat{J}_y$ is the collective spin operator, $\hat{x}$ ($\hat{p}$) is the position (momentum) operator of the collective vibrational mode. The pair $(F(t), G(t))$ traverses a circular loop in the mechanical phase space. At times when the loop is closed, only the first term in $\hat{U}(t)$ is left and $A(t)$ equals the enclosed area of the circle. The gate is thus independent of the state of the vibrational mode. The Milburn gate [3] uses bichromatic laser fields on resonance with the two sidebands of the vibrational motion of the ions. By properly choosing the phases of a sequence of laser pulses, the gate becomes $\hat{U} = \exp(i\kappa_x\hat{x}\hat{J}_z)\exp(i\kappa_p\hat{p}\hat{J}_z)\exp(-i\kappa_x\hat{x}\hat{J}_z)\exp(-i\kappa_p\hat{p}\hat{J}_z) = \exp(-i\kappa_x\kappa_p\hat{J}_z^2)$. It corresponds to a closed rectangle in the mechanical phase space. Similar to the Sørensen-Mølmer gate, the gate is independent of the vibrational motion.

III. GENERALIZATION OF THE MILBURN GATE

The original Milburn gate [3] describes a series of four pulsed interactions, forming a closed rectangle in the mechanical phase space. Here we generalize it to an arbitrary number of pulses, without the requirement of closing the mechanical-phase-space trajectory. We consider the case of equal interaction strength for each pulse and equal phase angle difference between adjacent pulses,

$$\begin{aligned}\hat{U}_p &= \exp\left(i\lambda\hat{O}\frac{1}{\sqrt{2}}(\hat{b}+\hat{b}^\dagger)\right)\exp\left(i\lambda\hat{O}\frac{1}{\sqrt{2}}(\hat{b}e^{i\theta}+\hat{b}^\dagger e^{-i\theta})\right)\\ &\times\exp\left(i\lambda\hat{O}\frac{1}{\sqrt{2}}(\hat{b}e^{i2\theta}+\hat{b}^\dagger e^{-i2\theta})\right)\times\cdots\\ &\times\exp\left(i\lambda\hat{O}\frac{1}{\sqrt{2}}(\hat{b}e^{i(N_p-1)\theta}+\hat{b}^\dagger e^{-i(N_p-1)\theta})\right)\\ &= \exp[i\hat{O}(c_1\hat{x}_m - c_2\hat{p}_m)]\exp(i\hat{O}^2c_3), \qquad (1)\end{aligned}$$

where $\hat{O}$ is an operator for the target mode, N_p is the number of pulses, λ is the dimensionless interaction strength, $\hat{b}$ ($\hat{b}^\dagger$) is the annihilation (creation) operator on the auxiliary mechanical mode, and θ is the phase angle increment. The second equality is a closed-form expression resulting from the Baker-Campbell-Hausdorff formula [20], where $c_1 = \sum_{n=0}^{N_p-1}\cos(n\theta)$, $c_2 = \sum_{n=0}^{N_p-1}\sin(n\theta)$, and $\hat{x}_m$ and $\hat{p}_m$ are the dimensionless position and momentum operator of the mechanical mode, respectively, with $\hat{x}_m = (\hat{b}+\hat{b}^\dagger)/\sqrt{2}$ and $\hat{p}_m = i(\hat{b}^\dagger-\hat{b})/\sqrt{2}$. The explicit expressions of c_1, c_2, and c_3 are shown in Appendix A.

We associate geometric meanings with the coefficients c_1, c_2, and c_3, as shown in Fig. 1. Each pulse in Eq. (1) is depicted as a thick black vector $\overrightarrow{V_iV_{i+1}}$ with length λ. The phase angle increment θ is the angle between two adjacent vectors. All the start and end points of the vectors lie on a circle, with its center labeled as R. The red dotted vector $\overrightarrow{V_1V_{N_p+1}}$ connects the start point of the first vector and the end point of the last vector. Its component on the X axis is c_1 and its component on the $-P$ axis is c_2; c_3 is the difference between the two areas. The first is N_p times the area of the triangle $\Delta V_iV_{i+1}R$. The second is the signed area of the triangle $\Delta V_1RV_{N_p+1}$. We define the net swept angle θ_{net} as $\theta_{\text{net}} = N_p\theta - 2M\pi$, with M a non-negative integer so that $0 \leqslant \theta_{\text{net}} < 2\pi$. If $\theta_{\text{net}} < \pi$ ($>\pi$), the positive (negative) sign is taken. These two situations are plotted in Figs. 1(a) and 1(b), respectively, for the simple case of $M = 0$. Note that if the mechanical-phase-space trajectories displayed here by the thick black vectors are rotated counterclockwise around the coordinate center by 90°, they become the same as the phase-space trajectory defined by the unitary transformation of operators $\hat{U}^\dagger\hat{x}_m\hat{U} = \exp[-i(c_1\hat{x}_m - c_2\hat{p}_m)]\hat{x}_m\exp[i(c_1\hat{x}_m - c_2\hat{p}_m)] = \hat{x}_m + c_2$ and $\hat{U}^\dagger\hat{p}_m\hat{U} = \exp[-i(c_1\hat{x}_m - c_2\hat{p}_m)]\hat{p}_m\exp[i(c_1\hat{x}_m - c_2\hat{p}_m)] = \hat{p}_m + c_1$.

IV. SØRENSEN-MØLMER GATE AS THE CONTINUOUS LIMIT OF THE MILBURN GATE

The continuous regime can be derived by taking the continuous limit of the pulsed regime. To be specific, we define the rescaled interaction strength $k = \lambda/\sqrt{2}\theta$ and take the limits $\theta \to 0$ and $N_p \to \infty$ while keeping the product $N_p\theta = \phi$ constant, with the angle ϕ proportional to the interaction time $\phi = \omega_m t$, where ω_m is the frequency of the mechanical mode. The resulting gate becomes

$$\hat{U}_c = \exp[i\hat{O}(d_1\hat{x}_m - d_2\hat{p}_m)]\exp(i\hat{O}^2d_3), \qquad (2a)$$

$$d_1 = \sqrt{2}k\sin\omega_m t, \qquad (2b)$$

$$d_2 = \sqrt{2}k(1-\cos\omega_m t), \qquad (2c)$$

$$d_3 = k^2(\omega_m t - \sin\omega_m t). \qquad (2d)$$

This is in the form of a continuous interaction given by the Sørensen-Mølmer gate [5]. The coefficients d_1, d_2, and d_3 also have geometric meanings, as shown in Fig. 2. The continuous interaction is represented by the thick black arc with the start point L_1 at the coordinate center and the end point L_2 on a circle with radius $\sqrt{2}k$ whose center R is on the $-P$ axis. The angle swept by $|L_2R|$ from $|L_1R|$ is ϕ. The $X(-P)$ component of the red dotted vector $\overrightarrow{L_1L_2}$ equals d_1 (d_2); d_3 is given by the difference between the two areas. Suppose $\phi = 2\pi M + \phi_{\text{net}}$, where M is a non-negative integer and $0 \leqslant \phi_{\text{net}} < 2\pi$. The first area is the area of M circles plus the area of the circular sector formed by the arc L_1L_2 and the two radii $|L_1R|$ and $|L_2R|$, with central angle ϕ_{net}. The second area is the signed area of the triangle ΔL_1RL_2, taking a positive (negative) sign for $\phi_{\text{net}} < \pi$ ($>\pi$). Figure 2 shows the two cases for $M = 0$.

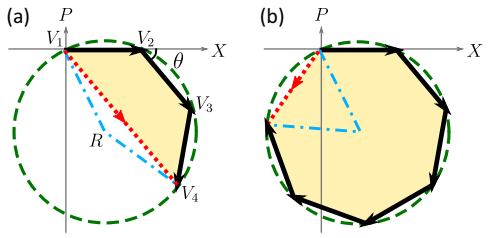

FIG. 1. Geometric explanation of the Milburn gate in the mechanical phase space for (a) $\theta_{\rm net} < \pi$ and (b) $\theta_{\rm net} > \pi$. The $X(-P)$ component of the red dotted vector represents c_1 (c_2) and the area of the yellow shaded region represents c_3.

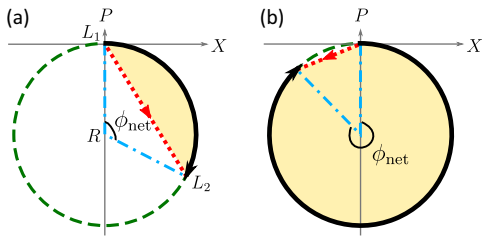

FIG. 2. Geometric explanation of the Sørensen-Mølmer gate in the mechanical phase space for (a) $\phi_{\rm net} < \pi$ and (b) $\phi_{\rm net} > \pi$. The X $(-P)$ component of the red dotted vector represents d_1 (d_2) and the area of the yellow shaded region represents d_3.

V. INCLUDING RELATIVE ERROR

Both the Sørensen-Mølmer gate and the Milburn gate have the property that if the mechanical-phase-space trajectory forms a closed loop, the gate operator becomes independent of the mechanical oscillator mode, thus removing the necessity of mechanical cooling. However, any error in parameters of the gate will violate this condition, entangling the target mode and the auxiliary mechanical mode. As shown in Figs. 1 and 2, the amount of entanglement is quantified by the length of the red dotted vector, which is bound to the green dashed circle. A straightforward strategy to suppress the amount of entanglement is to reduce the interaction strength and in compensation traverse the mechanical phase space multiple times, an idea originating from the weak-field coupling regime in Ref. [5]. However, the way the gate fidelity is affected by this transformation is not straightforward. In this section we first study the Sørensen-Mølmer gate when there is relative error in controlling the interaction time. We then study the Milburn gate when there is error in the phase angle increment θ. Finally, we discuss a way of unifying the two results in one mathematical framework.

A. Relative error in interaction time for the Sørensen-Mølmer gate

It is straightforward to deduce from the Sørensen-Mølmer gate expression (2) that no entanglement between the target mode and the mechanical mode is generated if $\omega_m t = 2K\pi$, with K a positive integer. For simplicity, we assume $K = 1$. Generalization to other values of K is straightforward. Consider the case that the interaction time t' cannot be controlled precisely so that $t' = (1+\eta)2\pi/\omega_m$. Here η characterizes the relative error of the interaction time, $|\eta| \ll 1$. The gate can be decomposed into $\hat{U}_{c,N=1}(\eta) = \hat{V}_{m,N=1}\hat{V}_{O,N=1}\hat{U}_{c,T}$, where $\hat{V}_{m,N=1}$ is the error gate induced by entanglement with the mechanical mode, $\hat{V}_{O,N=1}$ is the error gate induced by an effective additional self-interaction, and $\hat{U}_{c,T}$ is the target gate. The explicit expressions are listed in Appendix A and also correspond to Eqs. (3) below, taking $N = 1$. For $|\eta| \ll 1$, $\hat{V}_{O,N=1}$ is approximately the identity operator. This can be understood from Fig. 2. For simplicity, suppose $\eta > 0$; then $\phi_{\rm net} = 2\pi\eta$ [Fig. 2(a)]. The yellow shaded area is proportional to the exponent of $\hat{V}_{O,N=1}$, which is proportional to $O(\eta^2)$.

Consider reducing the interaction strength by a factor of N, $k \to k/N$. In order to reproduce the same target gate, the interaction time needs to increase by a factor of N^2, $t' \to N^2 t'$. The gate becomes

$$\hat{U}_{c,N}(\eta) = \hat{V}_{m,N}\hat{V}_{O,N}\hat{U}_{c,T}, \tag{3a}$$

$$\hat{V}_{m,N} = \exp\left(i\sqrt{2}\frac{k}{N}\hat{O}\{\sin(\eta 2\pi N^2)\hat{x}_m - [1-\cos(\eta 2\pi N^2)]\hat{p}_m\}\right), \tag{3b}$$

$$\hat{V}_{O,N} = \exp\left[ik^2\hat{O}^2\left(\eta 2\pi - \frac{\sin(\eta 2\pi N^2)}{N^2}\right)\right], \tag{3c}$$

$$\hat{U}_{c,T} = \exp(ik^2\hat{O}^2 2\pi), \tag{3d}$$

with η the same relative error of the interaction time as before. The target mode gets completely disentangled from the mechanical mode for all values of $|\eta| \ll 1$ if the limit $N \to \infty$ is taken, where the gate turns out to be $\hat{U}_{c,N\to\infty}(\eta) = \hat{V}_{O,N\to\infty}\hat{U}_{c,T}$, with $\hat{V}_{O,N\to\infty} = \exp(ik^2\hat{O}^2\eta 2\pi)$. Note that $\hat{V}_{O,N\to\infty}$ is not an identity operator, indicating a finite error in the self-interaction.

Whether reducing the interaction strength together with increasing the interaction time improves the gate fidelity depends on the comparison between the impact of $\hat{V}_{m,N=1}$ and $\hat{V}_{O,N\to\infty}$. For instance, if the mechanical mode is initially in a high-temperature thermal state, $\hat{V}_{m,N=1}$ dominates $\hat{V}_{O,N\to\infty}$. The transformation improves the fidelity. In contrast, the purity of the target mode always increases after the transformation, regardless of the relative impact of $\hat{V}_{m,N=1}$ and $\hat{V}_{O,N\to\infty}$.

B. Error in phase angle increment for the Milburn gate

The Milburn gate (1) forms a regular polygon in the mechanical phase space if $\theta = 2\pi/N_p$, under which condition the target mode disentangles from the mechanical mode. The target gate is therefore

$$\hat{U}_{p,T} = \exp\left[i\lambda^2\hat{O}^2\frac{N_p}{4}\cot\left(\frac{\pi}{N_p}\right)\right]. \tag{4}$$

Note that, for simplicity, we have assumed that the mechanical phase space is traversed once.

We consider an error in controlling the phase angle increment θ. This is also an error in controlling time if the phase angle increment is implemented by leaving the mechanical oscillator mode to evolve freely for a certain amount of time, as in a pulsed optomechanical system, which we will discuss

later [19]. Suppose the phase angle increment is $\theta' = (1+\xi)2\pi/N_p$, where ξ is the relative error satisfying $|\xi| \ll 1$. The mechanical-phase-space trajectory becomes open, indicating entanglement between the two modes. Similar to the idea in the Sørensen-Mølmer gate, the entanglement decreases after reducing the interaction strength $\lambda \to \lambda/N$ together with increasing the number of pulses $N_p \to N^2 N_p$, for N a positive integer. Note that θ' is not changed by this transformation. The mechanical phase space is traversed multiple times and the gate becomes

$$\hat{U}_{p,N}(\xi) = \exp(i\hat{\psi}_{m,N})\exp(i\hat{\psi}_{O,N})\hat{U}_{p,T}, \tag{5a}$$

$$\begin{aligned}\hat{\psi}_{m,N} = \frac{\lambda}{N}\hat{O}\Bigg\{&\left[\frac{1}{2}+\frac{1}{2}\cos\left(N^2\xi 2\pi - \frac{2\pi}{N_p} - \xi\frac{2\pi}{N_p}\right) + \frac{1}{2}\sin\left(N^2\xi 2\pi - \frac{2\pi}{N_p} - \xi\frac{2\pi}{N_p}\right)\cot\left(\frac{\pi}{N_p}+\xi\frac{\pi}{N_p}\right)\right]\hat{x}_m \\ &-\left[\frac{1}{2}\cot\left(\frac{\pi}{N_p}+\xi\frac{\pi}{N_p}\right) + \frac{1}{2}\sin\left(N^2\xi 2\pi - \frac{2\pi}{N_p} - \xi\frac{2\pi}{N_p}\right)\right. \\ &\left.-\frac{1}{2}\cos\left(N^2\xi 2\pi - \frac{2\pi}{N_p} - \xi\frac{2\pi}{N_p}\right)\cot\left(\frac{\pi}{N_p}+\xi\frac{\pi}{N_p}\right)\right]\hat{p}_m\Bigg\},\end{aligned} \tag{5b}$$

$$\hat{\psi}_{O,N} = \lambda^2\hat{O}^2\left\{\frac{N_p}{4}\left[\cot\left(\frac{\pi}{N_p}+\xi\frac{\pi}{N_p}\right) - \cot\left(\frac{\pi}{N_p}\right)\right] - \frac{\sin(N^2\xi 2\pi)}{8N^2\sin^2\left(\frac{\pi}{N_p}+\xi\frac{\pi}{N_p}\right)}\right\}. \tag{5c}$$

To check whether the transformation of reducing the interaction strength together with increasing the number of pulses improves the gate performance, we compare the error gates of the original gate ($N = 1$) and the limit $N \to \infty$. Here $\exp(i\hat{\psi}_{m,N\to\infty})$ is an identity operator, but $\exp(i\hat{\psi}_{m,N=1})$ is not. Therefore, the purity of the target mode always increases as N increases. Taylor expansion of $\hat{\psi}_{O,N=1}$ in terms of ξ, keeping up to the linear term, leads to

$$\hat{\psi}_{O,N=1} \approx -\lambda^2\hat{O}^2\frac{\pi\xi}{2\sin^2\left(\frac{\pi}{N_p}\right)}. \tag{6}$$

Note that this is different from the case of the Sørensen-Mølmer gate, where the effective additional self-interaction is zero to the first order of the relative error. It is because here both the central angle and the radius of the circle change with the phase angle increment θ' [Fig. 1(a)]. Similarly, Taylor expansion of $\hat{\psi}_{O,N\to\infty}$ gives

$$\hat{\psi}_{O,N\to\infty} \approx -\lambda^2\hat{O}^2\frac{\pi\xi}{4\sin^2\left(\frac{\pi}{N_p}\right)}. \tag{7}$$

The effective additional self-interaction is thus also reduced by the transformation. As a result, the fidelity of the Milburn gate is expected to improve under this transformation.

C. Unifying the two schemes

A natural question arises here. Given that the Sørensen-Mølmer gate is the continuous limit of the Milburn gate, as demonstrated in Sec. IV, why do the fidelities of the two gates behave differently in the presence of relative error and upon the transformation of decreasing the interaction strength together with traversing the phase space multiple times?

After examining the continuous limit of the Milburn gate [see the paragraph above Eq. (2)], we point out that Eq. (3) is indeed the continuous limit of Eq. (5). To be specific, if we replace the interaction strength λ in Eq. (5) with

$$\lambda = \sqrt{2}k(1+\xi)\frac{2\pi}{N_p} \tag{8}$$

and take the limit $N_p \to \infty$, we get Eq. (3) after renaming ξ as η. Note that in Eq. (8), λ explicitly depends on the relative error ξ. This dependence results in the difference between $\exp(i\hat{\psi}_{O,N=1})$ and $\hat{V}_{O,N=1}$ and the difference between $\exp(i\hat{\psi}_{O,N\to\infty})$ and $\hat{V}_{O,N\to\infty}$. Indeed, if we insert Eq. (8) into the error estimations for the Milburn gate [Eqs. (6) and (7)] and expand to first order in ξ, we recover the error estimation for the Sørensen-Mølmer gate. In Appendix A we use a diagram to show how the expressions in the two regimes are related to each other via equalities and limits.

Equation (8), together with the original rescaling relation $\lambda = \sqrt{2}k\theta$ above Eq. (2), connects the pulsed-interaction regime with the continuous-interaction regime. This unification will be further illustrated with an example in optomechanics.

VI. OPTOMECHANICAL MODEL AS AN EXAMPLE

We have already discussed the general abstract form of the Milburn gate and the Sørensen-Mølmer gate. We focused on the presence of a relative error in the gate implementation. For the Sørensen-Mølmer gate, we considered the error in the gate implementation time, while for the Milburn gate, we considered the error in the phase angle increment. We analyzed the performance of the gates if we decrease the interaction strength and traverse the mechanical phase space multiple times. The latter refers to increasing the interaction time for the Sørensen-Mølmer gate and increasing the number of pulses for the Milburn gate. In this section we apply our results to an optomechanical system (see Fig. 3), where the Sørensen-Mølmer gate corresponds to the continuous-interaction regime and the Milburn gate corresponds to the pulsed-interaction regime. We will also show that the phase angle increment in the Milburn gate is also related to an evolution time. Additionally, we take the dissipation of the mechanical oscillator into account. By deriving the analytical solutions, we further comment on the relations between the Milburn gate and the Sørensen-Mølmer gate.

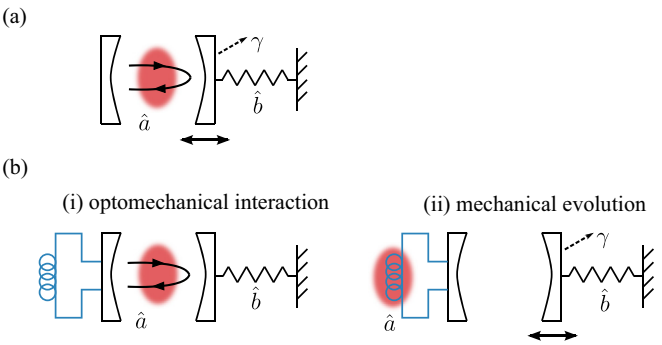

FIG. 3. The optomechanical model is illustrated as a Fabry-Pérot cavity here. The optical field circulates inside the cavity (red circle, described by the annihilation operator $\hat{a}$), one end mirror of which is movable and modeled as a mechanical oscillator (annihilation operator $\hat{b}$). The optical field exerts a radiation pressure on the mechanical oscillator, while the mechanical oscillator modifies the optical path of the field. (a) In the continuous-interaction regime, the optical field stays in the cavity for multiple mechanical periods. The optomechanical interaction happens simultaneously with the free evolution of the mechanical oscillator (double-headed arrow) and the possible mechanical dissipation (dashed arrow, γ as the dissipation rate). (b) In the pulsed-interaction regime, there are two separate steps that are repeated periodically. (i) The first step is the optomechanical interaction. It is on a much shorter timescale than the mechanical period; therefore, in this step both the mechanical oscillator free evolution and dissipation are neglected. (ii) In the second step, the optical field exits the cavity to enter a delay line (illustrated as the blue circuit). The mechanical oscillator, at the same time, evolves freely for a fraction of the mechanical period, together with the possible mechanical dissipation. The two steps are then repeated.

A. Unitary dynamics

We consider an example of an optomechanical system to analytically quantify the performance of the gates under the transformation described above. An optomechanical system consists of a Fabry-Pérot cavity with a movable mirror [13]. The light field inside the cavity interacts with the mechanical oscillation of the movable mirror via radiation pressure. The Hamiltonian in the frame rotating with the field frequency is [17,18]

$$\hat{H} = \hbar\omega_m \hat{b}^\dagger \hat{b} - \hbar g_0 \hat{a}^\dagger \hat{a} \frac{\hat{b}^\dagger + \hat{b}}{\sqrt{2}}, \tag{9}$$

where g_0 is the optomechanical interaction strength and $\hat{a}$ ($\hat{a}^\dagger$) is the annihilation (creation) operator of the field.

If the cavity photon decay rate κ is small, the field is kept in the cavity for multiple mechanical periods and the system is in the continuous-interaction regime [see Fig. 3(a)]. The time-evolution operator is thus calculated to be [21]

$$\begin{aligned}\hat{U}_{c,1}^{(\mathrm{om})}(t) &= e^{-i\hat{H}t/\hbar} \\ &= \exp\left(i\frac{g_0}{\omega_m}\hat{a}^\dagger\hat{a}\{\sin(\omega_m t)\hat{x}_m - [1-\cos(\omega_m t)]\hat{p}_m\}\right) \\ &\quad \times \exp\left(i\frac{g_0^2}{2\omega_m^2}(\hat{a}^\dagger\hat{a})^2[\omega_m t - \sin(\omega_m t)]\right) \\ &\quad \times \exp(-i\omega_m t\hat{b}^\dagger\hat{b}).\end{aligned} \tag{10}$$

The last term induces a uniform rotation in the mechanical phase space. It has no effect if the mechanical mode is initially in a thermal state, which is the case we will focus on. Here $\hat{U}_{c,1}^{(\mathrm{om})}(t)$ is in the form of the Sørensen-Mølmer gate with dimensionless interaction strength $k = g_0/\sqrt{2}\omega_m$ and $\hat{O} = \hat{a}^\dagger\hat{a}$.

As in Sec. V A, suppose that the target gate corresponds to the interaction time $t = 2\pi/\omega_m$ and there is a relative error in the actual interaction time so that $t' = (1+\eta)t$. We investigate the change in gate performance as we reduce the interaction strength $k \to k/N$ and increase the interaction time $t' \to N^2 t'$. The initial state of the field is assumed to be a coherent state $|\alpha\rangle_f$. The mechanical oscillator is initialized to a thermal state with mean phonon number n_{th}. Following the discussion in Sec. V A, the purity of the final field state is improved by taking a large value of N. The fidelity depends on the comparison between $\hat{V}_{m,N=1}$ and $\hat{V}_{O,N\to\infty}$. We consider the change of the mean value of the field quadrature operator induced by these two error gates, which is the lowest-order contribution. Suppose α is real without loss of generality. For $\hat{V}_{m,N=1}$,

$$\begin{aligned}&\langle\hat{V}_{m,N=1}^\dagger(\hat{a}e^{-i\varphi} + \hat{a}^\dagger e^{i\varphi})\hat{V}_{m,N=1}\rangle \\ &\quad = 2\alpha\cos\varphi\exp\{-(2n_{\mathrm{th}}+1)k^2[1-\cos(\eta 2\pi)]\},\end{aligned} \tag{11}$$

inducing a decay of the field quadrature amplitude. For $\hat{V}_{O,N\to\infty}$,

$$\begin{aligned}&\langle\hat{V}_{O,N\to\infty}^\dagger(\hat{a}e^{-i\varphi} + \hat{a}^\dagger e^{i\varphi})\hat{V}_{O,N\to\infty}\rangle \\ &\quad = 2\alpha e^{-\alpha^2[1-\cos(4\pi\eta k^2)]}\cos[\varphi - \alpha^2\sin(4\pi\eta k^2) - 2\pi\eta k^2],\end{aligned} \tag{12}$$

resulting in both a decay in amplitude and a change in phase. For practical optomechanical parameters of solid-state systems [13], the amplitude decays in both cases are negligibly small. It is thus expected that the change in the effective self-interaction induced by $\hat{V}_{O,N\to\infty}$ dominates the effect of $\hat{V}_{m,N=1}$. The transformation of reducing the interaction strength together with increasing the interaction time reduces the fidelity of the field state.

Figure 4 shows an example of the gate performance under the transformation. We choose the amplitude of the coherent state $\alpha = 100$, the dimensionless interaction strength $k = 0.001$, and the thermal state with mean phonon number $n_{\mathrm{th}} = 100$. Figure 4(a) depicts the Q function of the field state, $Q(\beta) = {}_f\langle\beta|\rho_f|\beta\rangle_f/\pi$. Figure 4(a i) is for the target state. It represents a self-Kerr interaction on a coherent state, inducing rotation and a small amount of squeezing [18,22]. Figure 4(a ii) is for the field state at time $t' = (1+\eta)2\pi/\omega_m$ with $\eta = 0.05$. Entanglement with the thermal mechanical mode smears out the peak of the Q function, while the center of the peak remains unchanged. Figure 4(a iii) is for $t' = N^2(1+\eta)2\pi/\omega_m$ and dimensionless interaction strength k/N with $\eta = 0.05$ and $N = 4$. The extra rotation induced by $\hat{V}_{O,N=4}$ is clear. Figure 4(a iv) is for the limit $N \to \infty$ with $\eta = 0.05$. The field becomes disentangled from the mechanical oscillator, so the peak of the Q function is concentrated. However, the extra rotation means the overlap with the target state is smaller than that for $N = 1$. Figure 4(b) plots the fidelity of the final field state compared with the target state, as

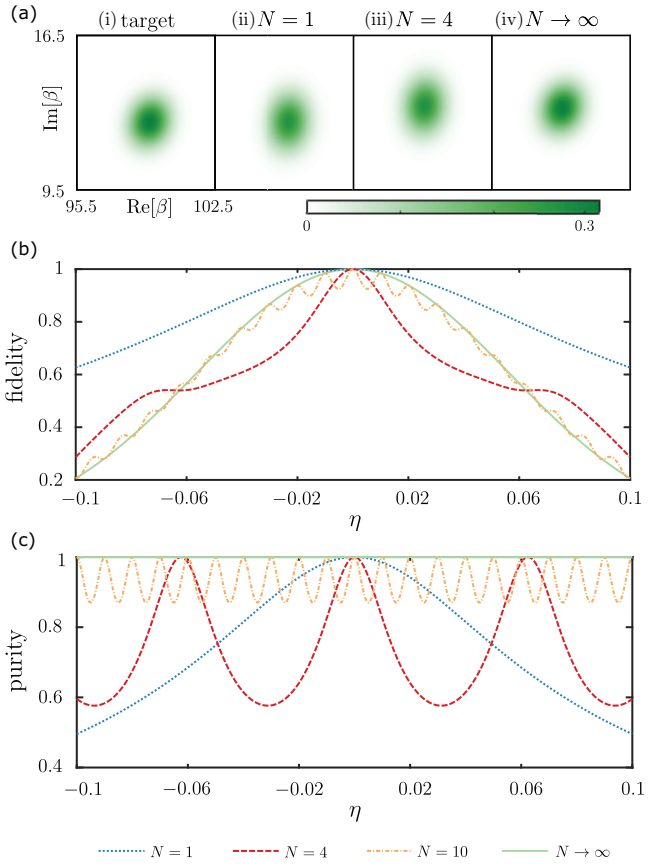

FIG. 4. Performance of the Sørensen-Mølmer gate (continuous optomechanical interaction) for $\alpha = 100$, $k = 0.001$, and $n_{\text{th}} = 100$. (a) The Q function of the optical field for (i) the target state and (ii)–(iv) states with relative error in the interaction time $\eta = 0.05$ for different values of N: (ii) $N = 1$, (iii) $N = 4$, and (iv) $N \to \infty$. (b) Fidelity of the final field state compared with the target state as a function of η for different values of N. (c) Purity of the final field state as a function of η for different values of N. For (b) and (c), the blue dotted line is for $N = 1$, the red dashed line is for $N = 4$, the orange dot-dashed line is for $N = 10$, and the green solid line is for $N \to \infty$.

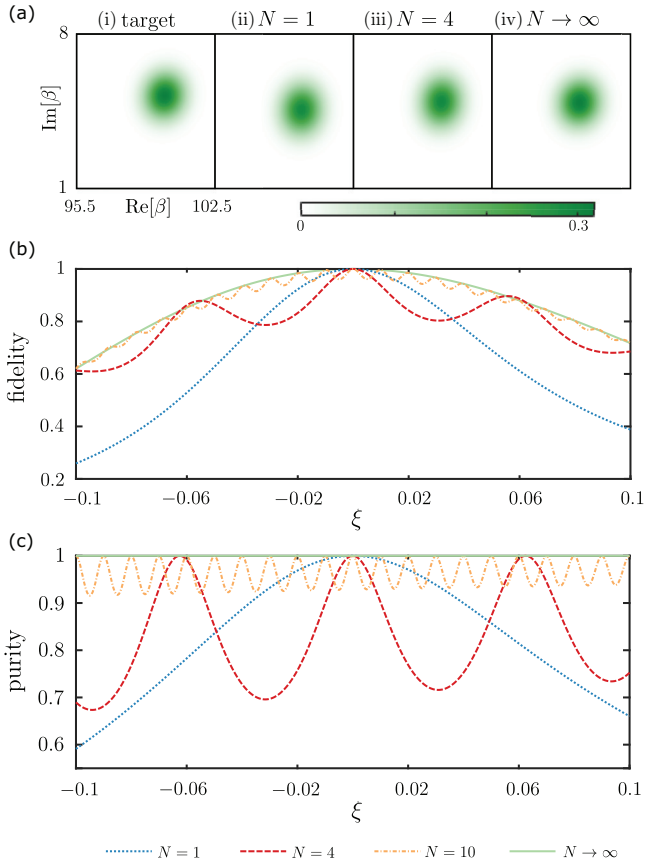

FIG. 5. Performance of the Milburn gate (pulsed optomechanical interaction) for $\alpha = 100$, $\lambda = 0.001$, $N_p = 6$, and $n_{\text{th}} = 100$. (a) The Q function of the field for (i) the target state and (ii)–(iv) states with relative error in the phase angle increment $\xi = 0.05$ for different values of N: (ii) $N = 1$, (iii) $N = 4$, and (iv) $N \to \infty$. (b) Fidelity of the final field state as a function of ξ for different N. (c) Purity of the final field state as a function of ξ for different N. The legend is the same as in Fig. 4.

a function of the relative error in interaction time η, for $N = 1$ (blue dotted line), $N = 4$ (red dashed line), $N = 10$ (orange dot-dashed line), and $N \to \infty$ (green solid line). The fidelity is defined as the overlap between the state of the field and the target state, which is

$$F_c = {}_f\langle\alpha|e^{-i2\pi k^2(\hat{a}^\dagger\hat{a})^2}\rho_f e^{i2\pi k^2(\hat{a}^\dagger\hat{a})^2}|\alpha\rangle_f. \tag{13}$$

As discussed before, the fidelity is reduced by the transformation due to the resultant error in the effective self-interaction. Note that $N = 10$ already approaches the limit $N \to \infty$. Figure 4(c) plots the purity of the final field state as a function of η, for the same values of N as in Fig. 4(b). The purity is defined as

$$P_c = \text{Tr}\left(\rho_f^2\right). \tag{14}$$

The purity is already largely improved for $N = 10$ and will reach 1 for any interaction time in the limit $N \to \infty$. The analytical expressions for the Q function, fidelity, and purity are shown in Appendix B.

If the cavity photon decay rate is large ($\kappa > \omega_m$), the optomechanical system is in the pulsed-interaction regime [16,17,19]. To be specific, the field enters the cavity and interacts with the mechanical oscillator only for a very short time. After that the field exits the cavity via a delay line such that both the field and the mechanical oscillator evolve freely without the optomechanical interaction [16]. Then the field reenters the cavity from the delay line to interact with the mechanical oscillator, which is a repetition of the initial step [see Fig. 3(b)]. This process in the frame rotating with the field frequency is described by the unitary evolution operator

$$\begin{aligned}\hat{U}_{p,1}^{(\text{om})}(N_p, \Delta t) &= \exp[i\lambda\hat{a}^\dagger\hat{a}(\hat{b}^\dagger + \hat{b})/\sqrt{2}]\exp(-i\omega_m\Delta t\hat{b}^\dagger\hat{b}) \\ &\times \exp[i\lambda\hat{a}^\dagger\hat{a}(\hat{b}^\dagger + \hat{b})/\sqrt{2}] \\ &\times \exp(-i\omega_m\Delta t\hat{b}^\dagger\hat{b}) \times \cdots \times \exp[i\lambda\hat{a}^\dagger\hat{a}(\hat{b}^\dagger + \hat{b})/\sqrt{2}].\end{aligned} \tag{15}$$

Here $\lambda = 2\pi g_0/\kappa$ is the effective coupling strength. The term $\exp[i\lambda\hat{a}^\dagger\hat{a}(\hat{b}^\dagger + \hat{b})/\sqrt{2}]$ is repeated N_p times. It describes the pulsed interaction between the field and the mechanical oscillator, where the free evolution of the mechanical oscillator is neglected due to the short time duration. The term $\exp(-i\omega_m\Delta t\hat{b}^\dagger\hat{b})$ is repeated $N_p - 1$ times. It describes the free evolution of the mechanical oscillator in between two pulsed interactions with the field, with Δt describing the time interval between the two pulsed interactions. Note that $\Delta t \gg 2\pi/\kappa$. It is straightforward to show that $\hat{U}^{(\mathrm{om})}_{p,1}(N_p, \Delta t) = \hat{U}_p \exp[-i\omega_m(N_p - 1)\Delta t\hat{b}^\dagger\hat{b}]$, where $\hat{U}_p$ is in the form of the Milburn gate (1) with $\hat{O} = \hat{a}^\dagger\hat{a}$, and $\theta = 2K_i\pi + \omega_m\Delta t$, with K_i an integer. For simplicity, we will assume that $K_i = 0$. The term $\exp[-i\omega_m(N_p - 1)\Delta t\hat{b}^\dagger\hat{b}]$ has no effect on the dynamics if the initial state of the mechanical oscillator is a thermal state.

Figure 5 shows the behavior of the pulsed optomechanical interaction, taking the initial field state as a coherent state $|\alpha = 100\rangle_f$, effective coupling strength $\lambda = 0.001$, and thermal phonon number $n_{\mathrm{th}} = 100$. The target gate is formed by $N_p = 6$ and $\theta = 2\pi/N_p$, corresponding to the mechanical-phase-space trajectory as a regular hexagon. As discussed in Sec. V B, suppose there is a relative error in the phase angle increment, $\theta' = (1 + \xi)\theta$, which corresponds to a small error in controlling the time interval Δt between two pulsed interactions. We consider the change in the gate performance when reducing λ to λ/N, increasing N_p to N^2N_p, and keeping θ' unchanged. The results in Fig. 5 clearly support the arguments in Sec. V B. The term $\exp(i\hat{\psi}_{m,N})$ entangles the optical field with the mechanical oscillator, causing a blurred peak of the Q function [Figs. 5(a ii)–5(a iv)] and reducing the purity [Fig. 5(c)]. Its effect reduces as N increases. The term $\exp(i\hat{\psi}_{O,N})$ represents an extra self-Kerr interaction, resulting in a rotation of the Q-function peak. The amount of rotation decreases as N increases [Fig. 5(a)], leading to a higher fidelity [Fig. 5(b)].

It is worth pointing out that for both the Sørensen-Mølmer gate (Fig. 4) and the Milburn gate (Fig. 5), when N is finite, the fast oscillation of the fidelity and purity as a function of the relative error implies that the corresponding curve does not stay above (or below) the curve of $N = 1$ for all values of the error. However, in the limit $N \to \infty$, the fast oscillation is smoothened. The two curves only intersect at the point with zero error. We can thus unambiguously define whether the gate performance is improved by the transformation independent of the value of the error.

B. Including the mechanical dissipation

Now we take into account an additional factor, which is the dissipation of the mechanical oscillator. This is relevant in the following way. An important property of both the Sørensen-Mølmer gate and the Milburn gate is that, under unitary dynamics, the state of the field is periodically disentangled from the mechanical oscillator. Therefore, the properties of the mechanical oscillator will not affect the state of the field at these times. However, the nonunitary dynamics of the mechanical oscillator will break the periodic disentanglement of the two modes, which is worth investigation.

The mechanical dissipation is included via the master equation in Lindblad form [14]

$$\frac{d\rho(t)}{dt} = -\frac{i}{\hbar}[\hat{H}_u, \rho(t)] + \frac{\gamma}{2}(2\hat{b}\rho(t)\hat{b}^\dagger - \hat{b}^\dagger\hat{b}\rho(t) - \rho(t)\hat{b}^\dagger\hat{b}), \tag{16}$$

where $\rho(t)$ is the joint state of the optical field and the mechanical oscillator, $\hat{H}_u$ is the Hamiltonian corresponding to the unitary dynamics, and γ is the rate of the mechanical dissipation. In writing down the master equation, we have assumed that the mechanical oscillator is in contact with a vacuum bath. For simplicity, we only consider the case where the initial state is a product state of the optical field in a coherent state and the mechanical oscillator in a vacuum state, namely,

$$\rho(0) = |\alpha\rangle_f\langle\alpha| \otimes |0\rangle_m\langle 0|. \tag{17}$$

As before, we assume α is real.

Let us start from the Milburn gate, which is the pulsed-interaction regime. The unitary dynamics without dissipation is described by Eq. (15). The mechanical dissipation only affects the steps where the mechanical oscillator evolves freely [see Fig. 3(b)], namely, the $\exp(-i\omega_m\Delta t\hat{b}^\dagger\hat{b})$ terms in Eq. (15). This is because the interaction time in the step of the pulsed optomechanical interaction [Fig. 3(b i)], $2\pi/\kappa$, is much smaller than the mechanical oscillator free evolution time Δt [Fig. 3(b ii)]. Making use of the transformation of the coherent state basis in the presence of the mechanical dissipation terms in Eq. (16) [23], the state of the system after N_p pulsed optomechanical interactions and $N_p - 1$ intervals containing mechanical dissipation is calculated to be

$$\rho_{N_p} = e^{-\alpha^2}\sum_{l_1,l_2=0}^{\infty}\frac{\alpha^{l_1+l_2}}{\sqrt{l_1!l_2!}}A_{N_p-1}(l_1, l_2)R_{N_p}(l_1, l_2)|l_1\rangle_f\langle l_2| \otimes |il_1\Phi_{N_p}\rangle_m\langle il_2\Phi_{N_p}|, \tag{18a}$$

$$\Phi_{N_p} = \frac{\lambda}{\sqrt{2}}\frac{1 - e^{(-i\omega_m\Delta t - \gamma\Delta t/2)N_p}}{1 - e^{-i\omega_m\Delta t - \gamma\Delta t/2}}, \tag{18b}$$

$$D = 1 - 2e^{-\gamma\Delta t/2}\cos(\omega_m\Delta t) + e^{-\gamma\Delta t}, \tag{18c}$$

$$\begin{aligned} A_{N_p-1}(l_1, l_2) = \exp\Bigg[-\frac{\lambda^2}{4}(l_1 - l_2)^2(1 - e^{-\gamma\Delta t})\frac{1}{D}\Bigg(N_p - 1 + \frac{e^{-\gamma\Delta t}(1 - e^{-(N_p-1)\gamma\Delta t})}{1 - e^{-\gamma\Delta t}} \\ - \frac{2}{D}\{e^{-\gamma\Delta t/2}\cos(\omega_m\Delta t) - e^{-\gamma\Delta t} - e^{-(\gamma/2)N_p\Delta t}\cos(N_p\omega_m\Delta t) \\ + e^{-(\gamma/2)(N_p+1)\Delta t}\cos[(N_p - 1)\omega_m\Delta t]\}\Bigg)\Bigg], \end{aligned} \tag{18d}$$

$$R_{N_p}(l_1,l_2)=\exp\Bigg[i\frac{\lambda^2}{2}\big(l_1^2-l_2^2\big)\Bigg(\frac{(N_p-1)e^{-\gamma\Delta t/2}\sin(\omega_m\Delta t)}{D}$$
$$-\frac{1}{D^2}\big\{e^{-\gamma\Delta t}\sin(2\omega_m\Delta t)-e^{-(\gamma/2)(N_p+1)\Delta t}\sin[(N_p+1)\omega_m\Delta t]$$
$$-2e^{-(3/2)\gamma\Delta t}\sin(\omega_m\Delta t)+2e^{-(\gamma/2)(N_p+2)\Delta t}\sin(N_p\omega_m\Delta t)$$
$$-e^{-(\gamma/2)(N_p+3)\Delta t}\sin[(N_p-1)\omega_m\Delta t]\big\}\Bigg)\Bigg], \tag{18e}$$

where the optical field state is expressed in the Fock-state basis and the mechanical oscillator state is expressed in the coherent state basis. Note that the exponent of $A_{N_p-1}(l_1,l_2)$ is purely real, while the exponent of $R_{N_p}(l_1,l_2)$ is purely imaginary. The state of the optical field is given by taking the partial trace over the mechanical oscillator,

$$\rho_{f,N_p}=\mathrm{Tr}_m(\rho_{N_p}). \tag{19}$$

As considered in Sec. VI A, we assume that there is a small error in controlling the interval time between two pulsed optomechanical interactions, namely, $\Delta t=(1+\xi)2\pi/N_p\omega_m$, with the relative error $|\xi|\ll 1$. We look into the performance of the gate if we reduce the interaction strength by a factor of N, $\lambda\to\lambda/N$, and increase the number of pulses by a factor of N^2, $N_p\to N^2N_p$, without changing Δt. We use the fidelity of the gate and the purity of the optical state to characterize the gate performance. The expressions are given in Appendix C. To visualize the results, we choose the initial coherent state amplitude of the optical field as $\alpha=100$, the effective optomechanical coupling strength $\lambda=0.001$, the number of pulses $N_p=6$, and the rescaled mechanical dissipation rate $\gamma/\omega_m=0.02$. The fidelity and purity as a function of the relative error ξ for different values of the factor N are plotted in Fig. 6. We can see that, for the chosen parameters, increasing the factor N improves both the fidelity and the purity, even after the dissipation of the mechanical oscillator is considered. For the fidelity of the gate, the presence of mechanical dissipation slightly smooths the oscillation of the fidelity as a function of the error ξ. For the purity of the final optical state, the presence of mechanical dissipation reduces the purity for each value of ξ and also smooths the oscillation of the purity as a function of ξ. Note that as we have taken the initial state of the mechanical oscillator as a vacuum state, the purity is much closer to 1 compared with the case in Sec. VI A. We have also chosen not to show the Q function, as the difference between different values of N turns out to be invisible.

The Sørensen-Mølmer gate, or equivalently the continuous-optomechanical-interaction regime, can be derived by taking the continuous limit of the Milburn gate, making use of the idea of Trotterization that is implicitly applied in Ref. [14]. To be specific, we first set both the pulsed-interaction time $2\pi/\kappa$ and the interval time Δt to a small time step dt. Then we take the limits $dt\to 0$ and $N_p\to\infty$, keeping the continuous-interaction time $t\equiv N_p dt$ finite. These two steps transform the system from the pulsed-interaction regime to the continuous-interaction regime. In other words, the continuous-interaction regime is described by inserting the Hamiltonian in Eq. (9) into $\hat{H}_u$ in the master equation (16). The continuous-time dynamics is decomposed into a series of infinitesimal time steps, each one with length dt. Within each dt, the optomechanical interaction, the mechanical oscillator free evolution, and the mechanical dissipation happen simultaneously [see Fig. 3(a)]. However, as dt is infinitesimal, the three processes can be separated into two sequential steps. The first one only contains the optomechanical interaction. The second one contains both the mechanical oscillator free evolution and the mechanical dissipation. This separation leads to a structure similar to the Milburn gate [see Fig. 3(b)]. Note that the difference with the Milburn gate is that, for the Milburn gate, the time for the mechanical oscillator free evolution and the mechanical dissipation, labeled as Δt, is finite.

For the continuous-interaction regime, the state of the system at time t is calculated by taking the continuous limit of the Milburn gate,

$$\rho(t)=e^{-\alpha^2}\sum_{l_1,l_2=0}^{\infty}\frac{\alpha^{l_1+l_2}}{\sqrt{l_1!l_2!}}A_t(l_1,l_2)R_t(l_1,l_2)|l_1\rangle_f\langle l_2|\otimes|il_1\Phi_t\rangle_m\langle il_2\Phi_t|, \tag{20a}$$

$$\Phi_t=\frac{g_0}{\sqrt{2}\big(i\omega_m+\frac{\gamma}{2}\big)}(1-e^{-(i\omega_m+\gamma/2)t}), \tag{20b}$$

$$A_t(l_1,l_2)=\exp\Bigg\{\frac{g_0^2}{4\omega_m^2+\gamma^2}(l_1-l_2)^2\Bigg[e^{-\gamma t}-1-\gamma t+\frac{4\gamma^2e^{-\gamma t/2}}{\gamma^2+4\omega_m^2}\Bigg(e^{\gamma t/2}-\cos\omega_m t+\frac{2\omega_m}{\gamma}\sin\omega_m t\Bigg)\Bigg]\Bigg\}, \tag{20c}$$

$$R_t(l_1,l_2)=\exp\Bigg[i\frac{2g_0^2}{4\omega_m^2+\gamma^2}\big(l_1^2-l_2^2\big)\Bigg(\omega_m t-e^{-\gamma t/2}\frac{4\omega_m^2-\gamma^2}{4\omega_m^2+\gamma^2}\sin\omega_m t-\frac{4\omega_m\gamma}{4\omega_m^2+\gamma^2}(1-e^{-\gamma t/2}\cos\omega_m t)\Bigg)\Bigg], \tag{20d}$$

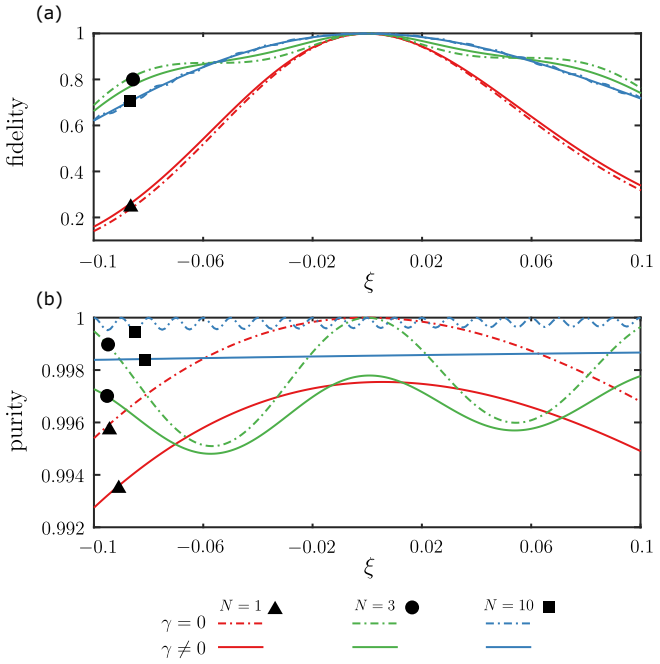

FIG. 6. Performance of the Milburn gate (pulsed optomechanical interaction) including the dissipation of the mechanical oscillator described by the Lindblad master equation, for $\alpha = 100$, $\lambda = 0.001$, $N_p = 6$, $n_{\rm th} = 0$, and $\gamma/\omega_m = 0.02$. (a) Fidelity of the final field state as a function of ξ for different N. (b) Purity of the final field state as a function of ξ for different N. Solid lines are for the cases with mechanical dissipation. For comparison, dot-dashed lines are for the cases without mechanical dissipation. The case of $N = 1$ is plotted in red and marked with triangles. The case of $N = 3$ is plotted in green and marked with circles. The case of $N = 10$ is plotted in blue and marked with squares.

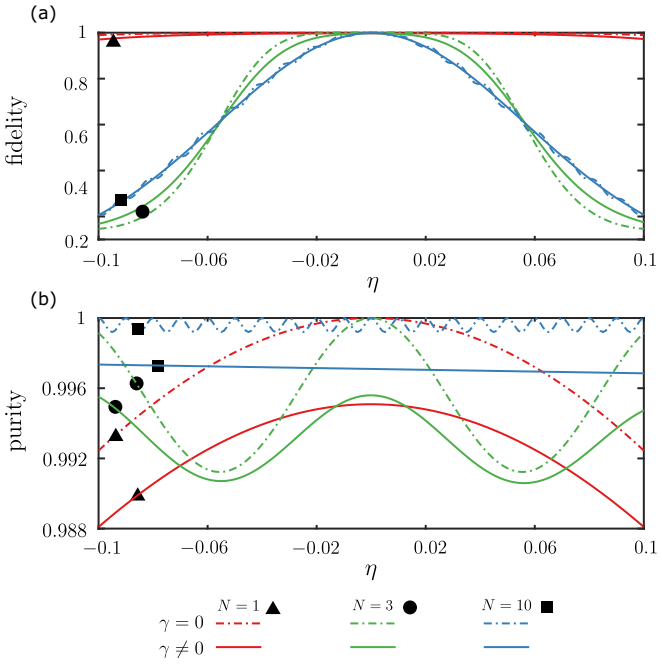

FIG. 7. Performance of the Sørensen-Mølmer gate (continuous optomechanical interaction) including the dissipation of the mechanical oscillator, described by Eq. (16), for $\alpha = 100$, $k = 0.001$, $n_{\rm th} = 0$, and $\gamma/\omega_m = 0.02$. (a) Fidelity of the final field state as a function of η for different N. (b) Purity of the final field state as a function of η for different N. The legend is the same as in Fig. 6.

where, as before, the optical field is expanded in the Fock-state basis and the mechanical oscillator is expanded in the coherent state basis. Similar to before, we consider that there is a small relative error in the evolution time, $t = (1 + \eta)2\pi/\omega_m$ for $|\eta| \ll 1$, causing the gate to be imperfect. We analyze how the gate performance changes if we reduce the optomechanical-interaction strength $g_0 \to g_0/N$ together with increasing the interaction time to $t = N^2(1 + \eta)2\pi/\omega_m$ for an integer N. The analytical expressions are given in Appendix C. We show an example of the results by choosing the parameters in the following way. The amplitude of the initial coherent state of the field is $\alpha = 100$, the dimensionless interaction strength is $k = g_0/\sqrt{2}\omega_m = 0.001$, and the rescaled mechanical dissipation rate is $\gamma/\omega_m = 0.02$. In Fig. 7 we plot the fidelity of the gate and the purity of the final optical state, as a function of the relative error η, for several values of N. For the chosen parameters, including mechanical dissipation does not change the qualitative responses of the gate to different values of N. Specifically, increasing the value of N only improves the purity of the final optical field [Fig. 7(b)], not the fidelity of the gate [Fig. 7(a)]. For each value of N, the comparison between the situations with and without mechanical dissipation is similar to the case of the Milburn gate. Including mechanical dissipation smooths the oscillations of the fidelity as a function of the relative error η. For the purity of the final optical state, mechanical dissipation has two effects. One is to reduce the purity for each value of η. The other is to smooth the oscillation of the purity as a function of η.

The unification of the pulsed-interaction scheme and the continuous-interaction scheme is clearly demonstrated in the example of an optomechanical system. On the one hand, we obtain the result for the continuous-interaction case [Eq. (20)] by taking the continuous limit of the pulsed interaction [see Eq. (18)]. This does not involve solving differential equations, as opposed to the method in Ref. [14]. On the other hand, the different behaviors of the two gates in the presence of the relative error in time, as plotted in Figs. 6 and 7, where the mechanical dissipation is included, can be unified by including the relative error in the Milburn gate interaction strength (8). We further comment on this in Appendix C, where analytical expressions are provided.

VII. CONCLUSION

Both the Sørensen-Mølmer gate and the Milburn gate are geometric phase gates on a target mode via interaction with one auxiliary mechanical oscillator mode. We have shown that the Sørensen-Mølmer gate is the continuous limit of the Milburn gate, including a geometrical explanation in the mechanical phase space. Both gates have the property that if the mechanical-phase-space trajectory is closed, the two modes disentangle, and thus the mechanical mode is only virtually involved. However, the performances of the gates are reduced in the presence of error in the gate parameters. We explicitly considered the error in time for the Sørensen-Mølmer gate and in the phase angle increment for the Milburn gate. The trans-

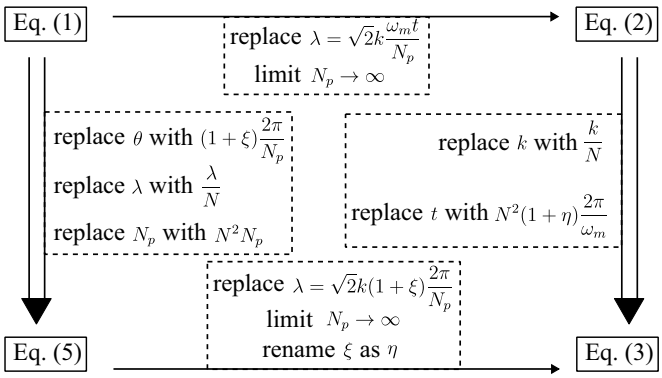

FIG. 8. Relations between the expressions in the pulsed-interaction regime and the continuous-interaction regime.

formation of decreasing the interaction strength together with increasing the number of loops traversed in the mechanical phase space can reduce the entanglement between the target mode and the mechanical oscillator mode, thus increasing the purity of the target mode. It increases the fidelity of the Milburn gate, but the fidelity of the Sørensen-Mølmer gate depends on the competition between thermal effect of the mechanical mode and error-induced additional self-interaction. We pointed out that the difference is because the interaction strength becomes dependent on the relative error when taking the continuous limit and once this dependence is taken into account, the behaviors of the two gates are understood in a single platform. We quantitatively illustrated this unification via an optomechanical system, where in addition we included the effect of the mechanical oscillator dissipation to emphasize the application of our unified framework.

ACKNOWLEDGMENTS

This work was supported by the KIST Open Research Program, the QuantERA ERA-NET within the EUs Horizon 2020 program, the UK Hub in Quantum Computing and Simulation with funding from UKRI EPSRC Grant No. EP/T001062/1, and the EPSRC (Grant No. EP/R044082/1) and the Royal Society. Y.M. was supported by the EPSRC Centre for Doctoral Training on Controlled Quantum Dynamics at Imperial College London (Grant No. EP/L016524/1) and funded by the Imperial College President's Ph.D. Scholarship.

APPENDIX A: ANALYTICAL EXPRESSIONS OF THE SØRENSEN-MØLMER GATE AND MILBURN GATE NOT INCLUDED IN THE MAIN TEXT

The explicit expressions of c_1, c_2, and c_3 in Eq. (1) are

$$c_1 = \lambda\left[\frac{1}{2} + \frac{1}{2}\cos[(N_p-1)\theta] + \frac{1}{2}\sin[(N_p-1)\theta]\cot\left(\frac{\theta}{2}\right)\right], \tag{A1a}$$

$$c_2 = \lambda\left[\frac{1}{2}\cot\left(\frac{\theta}{2}\right)\{1-\cos[(N_p-1)\theta]\} + \frac{1}{2}\sin[(N_p-1)\theta]\right], \tag{A1b}$$

$$c_3 = \frac{1}{2}\lambda^2\frac{N_p\sin\theta - \sin(N_p\theta)}{4\sin^2\left(\frac{\theta}{2}\right)}. \tag{A1c}$$

The expression of the Sørensen-Mølmer gate with relative error η in interaction time, for $N = 1$ (see Sec. V A), is

$$\hat{U}_{c,N=}(\eta) = \hat{V}_{m,N=1}\hat{V}_{O,N=1}\hat{U}_{c,T}, \tag{A2a}$$

$$\hat{V}_{m,N=1} = \exp\left(i\sqrt{2}k\hat{O}\{\sin(\eta 2\pi)\hat{x}_m - [1-\cos(\eta 2\pi)]\hat{p}_m\}\right), \tag{A2b}$$

$$\hat{V}_{O,N=1} = \exp\{ik^2\hat{O}^2[\eta 2\pi - \sin(\eta 2\pi)]\}, \tag{A2c}$$

$$\hat{U}_{c,T} = \exp(ik^2\hat{O}^2 2\pi). \tag{A2d}$$

In Fig. 8 we show how the expressions in the main text are connected to each other. The double-line arrow refers to an equality, while the single-line arrow refers to a limit. This figure represents the unified mathematical framework of the two gates.

APPENDIX B: ANALYTICAL EXPRESSIONS OF THE Q FUNCTION, FIDELITY, AND PURITY FOR UNITARY EVOLUTION OF THE OPTOMECHANICAL EXAMPLE

For the continuous-interaction regime, the Q function of the field state at time $t' = N^2(1+\eta)2\pi/\omega_m$ is (for real α)

$$Q_c(\beta) = \frac{1}{\pi}\sum_{l_1,l_2=0}^{\infty} e^{-\alpha^2-|\beta|^2}\frac{\alpha^{l_1+l_2}\beta^{*l_1}\beta^{l_2}}{l_1!l_2!}\Psi_c(l_1,l_2)M_c(l_1,l_2), \tag{B1a}$$

$$\Psi_c(l_1,l_2) = \exp\left(i\frac{k^2}{N^2}\left(l_1^2-l_2^2\right)[(1+\eta)2\pi N^2 - \sin(\eta 2\pi N^2)]\right), \tag{B1b}$$

$$M_c(l_1,l_2) = \exp\left(-\frac{k^2}{N^2}(l_1-l_2)^2(2n_{\rm th}+1)[1-\cos(\eta 2\pi N^2)]\right). \tag{B1c}$$

The fidelity is

$$F_c = \sum_{l_1,l_2=0}^{\infty} e^{-2\alpha^2}\frac{\alpha^{2(l_1+l_2)}}{l_1!l_2!}\exp\left[-i2\pi k^2\left(l_1^2-l_2^2\right)\right]\Psi_c(l_1,l_2)M_c(l_1,l_2). \tag{B2}$$

The purity is

$$P_c = \sum_{l_1,l_2=0}^{\infty} e^{-2\alpha^2}\frac{\alpha^{2(l_1+l_2)}}{l_1!l_2!}M_c^2(l_1,l_2). \tag{B3}$$

For the pulsed-interaction regime, the Q function of the field for the phase angle increment $\theta' = (1+\xi)2\pi/N_p$ is

$$Q_p(\beta) = \frac{1}{\pi}\sum_{l_1,l_2=0}^{\infty} e^{-\alpha^2-|\beta|^2}\frac{\alpha^{l_1+l_2}\beta^{*l_1}\beta^{l_2}}{l_1!l_2!}\Psi_p(l_1,l_2)M_p(l_1,l_2), \tag{B4a}$$

$$\Psi_p(l_1,l_2) = \exp\left(i\frac{\lambda^2}{N^2}\left(l_1^2-l_2^2\right)\frac{N^2N_p\sin[(1+\xi)2\pi/N_p]-\sin(N^2 2\pi\xi)}{8\sin^2[(1+\xi)\pi/N_p]}\right), \tag{B4b}$$

$$M_p(l_1,l_2) = \exp\left(-\frac{\lambda^2}{N^2}(l_1-l_2)^2(2n_{\rm th}+1)\frac{1-\cos(\xi 2\pi N^2)}{8\sin^2[(1+\xi)\pi/N_p]}\right). \tag{B4c}$$

The fidelity is

$$F_p = \sum_{l_1,l_2=0}^{\infty} e^{-2\alpha^2}\frac{\alpha^{2(l_1+l_2)}}{l_1!l_2!}\exp\left[-i\lambda^2\left(l_1^2-l_2^2\right)\frac{N_p}{4}\cot\left(\frac{\pi}{N_p}\right)\right]\Psi_p(l_1,l_2)M_p(l_1,l_2). \tag{B5}$$

The purity is

$$P_p = \sum_{l_1,l_2=0}^{\infty} e^{-2\alpha^2}\frac{\alpha^{2(l_1+l_2)}}{l_1!l_2!}M_p^2(l_1,l_2). \tag{B6}$$

APPENDIX C: ANALYTICAL EXPRESSIONS OF FIDELITY AND PURITY FOR THE OPTOMECHANICAL EXAMPLE INCLUDING MECHANICAL DISSIPATION

For the continuous-interaction regime, the fidelity for interaction time $t = N^2(1+\eta)2\pi/\omega_m$ is

$$\tilde{F}_c = \sum_{l_1,l_2=0}^{\infty} e^{-2\alpha^2}\frac{\alpha^{2(l_1+l_2)}}{l_1!l_2!}\exp\left[-i2\pi k^2\left(l_1^2-l_2^2\right)\right]\mathcal{P}_c(l_1,l_2)\mathcal{M}_c(l_1,l_2), \tag{C1a}$$

$$\mathcal{P}_c(l_1,l_2) = \exp\left[i\frac{4k^2\omega_m^2}{4\omega_m^2+\gamma^2}\left(l_1^2-l_2^2\right)\left((1+\eta)2\pi - \frac{1}{N^2}e^{-(\gamma/\omega_m)\pi(1+\eta)N^2}\frac{4\omega_m^2-\gamma^2}{4\omega_m^2+\gamma^2}\sin(\eta 2\pi N^2)\right.\right.$$
$$\left.\left. - \frac{1}{N^2}\frac{4\omega_m\gamma}{4\omega_m^2+\gamma^2}\left[1-e^{-(\gamma/\omega_m)\pi(1+\eta)N^2}\cos(\eta 2\pi N^2)\right]\right)\right], \tag{C1b}$$

$$\mathcal{M}_c(l_1,l_2) = \exp\left\{-\frac{k^2}{N^2}(l_1-l_2)^2\frac{4\omega_m^2}{4\omega_m^2+\gamma^2}\left[1-\cos(\eta 2\pi N^2)e^{-(\gamma/\omega_m)\pi(1+\eta)N^2} + \frac{\gamma}{\omega_m}\pi(1+\eta)N^2\right.\right.$$
$$\left.\left. - \frac{2\gamma^2}{\gamma^2+4\omega_m^2}e^{-(\gamma/\omega_m)\pi(1+\eta)N^2}\left(e^{(\gamma/\omega_m)\pi(1+\eta)N^2} - \cos(\eta 2\pi N^2) + \frac{2\omega_m}{\gamma}\sin(\eta 2\pi N^2)\right)\right]\right\}. \tag{C1c}$$

The purity is

$$\tilde{P}_c = \sum_{l_1,l_2=0}^{\infty} e^{-2\alpha^2} \frac{\alpha^{2(l_1+l_2)}}{l_1!l_2!} \mathcal{M}_c^2(l_1, l_2). \tag{C2}$$

Note that here we have chosen $n_{\text{th}} = 0$.

For the pulsed-interaction regime, the fidelity for phase angle increment $\theta = (1+\xi)2\pi/N_p$ is

$$\tilde{F}_p = \sum_{l_1,l_2=0}^{\infty} e^{-2\alpha^2} \frac{\alpha^{2l_1+2l_2}}{l_1!l_2!} \exp\left[-i\lambda^2(l_1^2 - l_2^2)\frac{N_p}{4}\cot\left(\frac{\pi}{N_p}\right)\right] \mathcal{P}_p(l_1, l_2)\mathcal{M}_p(l_1, l_2), \tag{C3a}$$

$$\mathcal{D} = 1 - 2e^{-\gamma(1+\xi)2\pi/2N_p\omega_m}\cos\left((1+\xi)\frac{2\pi}{N_p}\right) + e^{-\gamma(1+\xi)2\pi/N_p\omega_m}, \tag{C3b}$$

$$\begin{aligned}\mathcal{P}_p(l_1, l_2) = \exp\Bigg(i\frac{\lambda^2}{2N^2}(l_1^2 - l_2^2)\Bigg\{&\frac{1}{\mathcal{D}}(N^2N_p - 1)e^{-\gamma(1+\xi)2\pi/2N_p\omega_m}\sin\left((1+\xi)\frac{2\pi}{N_p}\right) - \frac{1}{\mathcal{D}^2}\Bigg[e^{-\gamma(1+\xi)2\pi/N_p\omega_m}\sin\left((1+\xi)\frac{4\pi}{N_p}\right)\\ &- e^{-(\gamma/2)(N^2N_p+1)(1+\xi)2\pi/N_p\omega_m}\sin\left(N^2 2\pi\xi + (1+\xi)\frac{2\pi}{N_p}\right) - 2e^{-(3/2)\gamma(1+\xi)2\pi/N_p\omega_m}\sin\left((1+\xi)\frac{2\pi}{N_p}\right)\\ &+ 2e^{-(\gamma/2)(N^2N_p+2)(1+\xi)2\pi/N_p\omega_m}\sin(N^2 2\pi\xi) - e^{-(\gamma/2)(N^2N_p+3)(1+\xi)2\pi/N_p\omega_m}\sin\left(N^2 2\pi\xi - (1+\xi)\frac{2\pi}{N_p}\right)\Bigg]\Bigg\}\Bigg),\end{aligned} \tag{C3c}$$

$$\begin{aligned}\mathcal{M}_p(l_1, l_2) = \exp\Bigg[-\frac{\lambda^2}{4N^2}(l_1 - l_2)^2\Bigg(&\frac{1}{\mathcal{D}}(1 - e^{-\gamma(1+\xi)2\pi/N_p\omega_m})\Bigg\{N^2N_p - 1 + \frac{e^{-\gamma(1+\xi)2\pi/N_p\omega_m}(1 - e^{-(N^2N_p-1)\gamma(1+\xi)2\pi/N_p\omega_m})}{1 - e^{-\gamma(1+\xi)2\pi/N_p\omega_m}}\\ &- \frac{2}{\mathcal{D}}\Bigg[e^{-\gamma(1+\xi)2\pi/2N_p\omega_m}\cos\left((1+\xi)\frac{2\pi}{N_p}\right) - e^{-\gamma(1+\xi)2\pi/N_p\omega_m} - e^{-(\gamma/2)N^2N_p(1+\xi)2\pi/N_p\omega_m}\cos(N^2 2\pi\xi)\\ &+ e^{-(\gamma/2)(N^2N_p+1)(1+\xi)2\pi/N_p\omega_m}\cos\left(N^2 2\pi\xi - (1+\xi)\frac{2\pi}{N_p}\right)\Bigg]\Bigg\}\\ &+ \frac{1}{\mathcal{D}}[1 - 2e^{-\gamma N^2N_p(1+\xi)2\pi/2N_p\omega_m}\cos(N^2 2\pi\xi) + e^{-\gamma N^2N_p(1+\xi)2\pi/N_p\omega_m}]\Bigg)\Bigg].\end{aligned} \tag{C3d}$$

The purity is

$$\tilde{P}_p = \sum_{l_1,l_2=0}^{\infty} e^{-2\alpha^2} \frac{\alpha^{2l_1+2l_2}}{l_1!l_2!} \mathcal{M}_p^2(l_1, l_2). \tag{C4}$$

The unification of the two gates in the presence of the mechanical dissipation can be shown in the following way. We insert Eq. (8) into $\mathcal{P}_p(l_1, l_2)$ and take the limit $N_p \to \infty$ to arrive at $\mathcal{P}_c(l_1, l_2)$. Similarly, we insert Eq. (8) into $\mathcal{M}_p(l_1, l_2)$ and take the limit $N_p \to \infty$ to arrive at $\mathcal{M}_c(l_1, l_2)$. The conversion from the purity $\tilde{P}_p$ to $\tilde{P}_c$ is therefore straightforward. For the fidelity $\tilde{F}_p$, in addition to the transforms of $\mathcal{P}_p(l_1, l_2)$ and $\mathcal{M}_p(l_1, l_2)$, we replace λ in the exponential factor $\exp[-i\lambda^2(l_1^2 - l_2^2)\frac{N_p}{4}\cot(\frac{\pi}{N_p})]$ with $\sqrt{2}k(2\pi/N_p)$. Note that this does not include the relative error ξ, as the exponential factor comes from the target state. Taking the limit $N_p \to \infty$ brings $\tilde{F}_p$ to $\tilde{F}_c$.

[1] G. S. Agarwal and R. Simon, Berry phase, interference of light beams, and the Hannay angle, Phys. Rev. A **42**, 6924 (1990).

[2] S. Chaturvedi, M. Sriram, and V. Srinivasan, Berry's phase for coherent states, J. Phys. A: Math. Gen. **20**, L1071 (1987).

[3] G. J. Milburn, Simulating nonlinear spin models in an ion trap, arXiv:quant-ph/9908037.

[4] A. Sørensen and K. Mølmer, Quantum Computation with Ions in Thermal Motion, Phys. Rev. Lett. **82**, 1971 (1999).

[5] A. Sørensen and K. Mølmer, Entanglement and quantum computation with ions in thermal motion, Phys. Rev. A **62**, 022311 (2000).

[6] G. Milburn, S. Schneider, and D. James, Ion trap quantum computing with warm ions, Fortschr. Phys. **48**, 801 (2000).

[7] C. A. Sackett, D. Kielpinski, B. E. King, C. Langer, V. Meyer, C. J. Myatt, M. Rowe, Q. Turchette, W. M. Itano, D. J. Wineland *et al.*, Experimental entanglement of four particles, Nature (London) **404**, 256 (2000).

[8] D. Leibfried, B. DeMarco, V. Meyer, D. Lucas, M. Barrett, J. Britton, W. M. Itano, B. Jelenković, C. Langer, T. Rosenband *et al.*, Experimental demonstration of a robust, high-fidelity geometric two ion-qubit phase gate, Nature (London) **422**, 412 (2003).

[9] A. Luis, Quantum mechanics as a geometric phase: Phase-space interferometers, J. Phys. A: Math. Gen. **34**, 7677 (2001).

[10] T. J. Proctor and V. Kendon, Hybrid quantum computing with ancillas, Contemp. Phys. **57**, 459 (2016).

[11] P. van Loock, W. J. Munro, K. Nemoto, T. P. Spiller, T. D. Ladd, S. L. Braunstein, and G. J. Milburn, Hybrid quantum computation in quantum optics, Phys. Rev. A **78**, 022303 (2008).

[12] T. P. Spiller, K. Nemoto, S. L. Braunstein, W. J. Munro, P. van Loock, and G. J. Milburn, Quantum computation by communication, New J. Phys. **8**, 30 (2006).

[13] M. Aspelmeyer, T. J. Kippenberg, and F. Marquardt, Cavity optomechanics, Rev. Mod. Phys. **86**, 1391 (2014).

[14] S. Bose, K. Jacobs, and P. L. Knight, Preparation of nonclassical states in cavities with a moving mirror, Phys. Rev. A **56**, 4175 (1997).

[15] K. Khosla, M. Vanner, W. Bowen, and G. Milburn, Quantum state preparation of a mechanical resonator using an optomechanical geometric phase, New J. Phys. **15**, 043025 (2013).

[16] I. Pikovski, M. R. Vanner, M. Aspelmeyer, M. S. Kim, and Č. Brukner, Probing Planck-scale physics with quantum optics, Nat. Phys. **8**, 393 (2012).

[17] F. Armata, L. Latmiral, I. Pikovski, M. R. Vanner, Č. Brukner, and M. S. Kim, Quantum and classical phases in optomechanics, Phys. Rev. A **93**, 063862 (2016).

[18] Y. Ma, F. Armata, K. E. Khosla, and M. S. Kim, Optical squeezing for an optomechanical system without quantizing the mechanical motion, Phys. Rev. Research **2**, 023208 (2020).

[19] M. R. Vanner, I. Pikovski, G. D. Cole, M. S. Kim, Č. Brukner, K. Hammerer, G. J. Milburn, and M. Aspelmeyer, Pulsed quantum optomechanics, Proc. Natl. Acad. Sci. USA **108**, 16182 (2011).

[20] J. J. Sakurai and J. Napolitano, *Modern Quantum Mechanics* (Pearson, Harlow, 2014), Vol. 185.

[21] S. Mancini, V. I. Man'ko, and P. Tombesi, Ponderomotive control of quantum macroscopic coherence, Phys. Rev. A **55**, 3042 (1997).

[22] G. J. Milburn, Quantum and classical Liouville dynamics of the anharmonic oscillator, Phys. Rev. A **33**, 674 (1986).

[23] D. F. Walls, M. J. Collet, and G. J. Milburn, Analysis of a quantum measurement, Phys. Rev. D **32**, 3208 (1985).